ARTICLE

Indigo@Silicalite: a New Organic−Inorganic Hybrid Pigment

Catherine Dejoie,[†] Pauline Martinetto,[*,†] Eric Dooryhée,[†,ǂ] Pierre Strobel,[†] Sylvie Blanc,[§] Patrice Bordat,[§] Ross Brown,[§] Florence Porcher,[∥,⊥] Manuel Sanchez del Rio,[#] and Michel Anne[†]

Institut Néel, UPR 2940 CNRS, 25 avenue des Martyrs, BP 166, F-38042 Grenoble Cedex 9, France, Institut Pluridisciplinaire de Recherche sur l'Environnement et les Matériaux (IPREM), UMR 5254 UPPA-CNRS, Hélioparc, 2 avenue Pierre Angot, F-64053 Pau Cedex 9, France, Laboratoire de Cristallographie, Résonnance Magnétique et Modélisation (CRM2), UHP-CNRS, Faculté des Sciences BP 70239, F- 54506 Vandoeuvre-les-Nancy, France, Laboratoire Léon Brillouin (LLB), UMR 12 CEA-CNRS, F-91191 Gif-sur-Yvette Cedex, France, European Synchrotron Radiation Facility (ESRF), 6 rue Jules Horowitz, F-38000 Grenoble, France, and National Synchrotron Light Source-II (NSLS-II), Brookhaven National Laboratory, Upton, New York 11973

ABSTRACT In the search for stable and enduring organic colors, we have combined indigo, a historical and industrially important chromophore, with silicalite, the MFI zeolite. The resulting pigment presents high color durability against most external agents (e.g., light, temperature). This stability and its physical properties are explained by the association of indigo with an inert mineral, which is also influenced by formation conditions such as the initial indigo concentration and the thermal treatment. The formation of the indigo@silicalite hybrid, particularly diffusion of the organic molecule, is monitored by optical spectroscopies, thermogravimetric measurements, and X-ray diffraction. Color stability is attested when indigo enters the pores of the zeolitic host, thus forming a new pigment with characteristics similar to those of Maya Blue. This opens the way to the low-cost engineering of metal-free, nonhazardous pigment powders based on indigoid and other dyes.

KEYWORDS: silicalite • zeolite • indigo • pigment • stability • UV−vis fluorescence • diffraction • color

I. INTRODUCTION

Long-lasting resistance of pigments to acids, alkalis, solvents, and biodegradants is an important issue in art and in the paint and pigment industries (1−4). In the quest for stable dyes, resistant to heat and moisture in particular, several organic−inorganic hybrids present good characteristics and are environmentally friendly as well: the color can be durably fixed by trapping or encapsulating an organic dye in a mineral or clay matrix (5, 6). Some of these hybrid pigments combine the properties of the microporous mineral substrate (chemical resistance, thermal and mechanical stability, harmlessness, etc.) and the color of the organic dye (7). The stability and appearance of such hybrid pigments are affected by both the structure of the host and the interactions between the host and dye (8, 9).

A particular organomineral system is indigo/silicalite. To our knowledge, this system has never been produced or studied. This new organic−inorganic pigment is inspired by the general features of the archeological pigment Maya Blue (5, 10), created by the ancient Mayan people by the mixing and heating of palygorskite or sepiolite clays with indigo dye. Despite certain controversy on the location of the indigo molecule within the clays (5, 11−15), a channel structure is known to be the key point to obtain a chemically and thermally stable dye. We thus copied the tubelike arrangement of the clay by using the silicalite zeolite as the inorganic matrix. Indigo is a blue dye well-known to ancient civilizations (16). Nowadays, the massive use of indigo (17) by the dye industry requires its transformation into a water-soluble (leuco) form (18). Indigo is the compound indigotin $C_{16}H_{10}N_2O_2$ [2-(1,3-dihydro-3-oxo-2*H*-indol-2-ylidene)-1,2-dihydro-3*H*-indol-3-one], a quasi-planar molecule of approximate dimensions 5 × 12 Å^2. In the present work, we consider using the naturally water-insoluble (keto) form of indigo for the formation of a stable pigment. Silicalite is a high silica zeolite belonging to the MFI family (19). Pure silicalite is exclusively formed by Si−O−Si bonds, which are responsible for its hydrophobic properties (20). In the presence of foreign atoms (Al, Ti, Fe, B, etc.) or structural defects, internal silanol groups contribute to the catalytic activities of this type of zeolite, used in industrial applications (21). The MFI structure may be described as a three-dimensional porous silicate with two interconnected tubular channel systems (19, 22). Sinusoidal channels with an opening of 5.1 × 5.5 Å^2 along the *a* axis ($P2_1/n$ space group) are intercon-

* To whom correspondence should be addressed. E-mail: pauline.martinetto@grenoble.cnrs.fr.
Received for review April 20, 2010 and accepted June 21, 2010
† Institut Néel.
ǂ NSLS-II.
§ IPREM.
∥ CRM2.
⊥ LLB.
ESRF.
DOI: 10.1021/am100349b
2010 American Chemical Society

Published on Web 07/20/2010

Table 1. Indigo@Silicalite Samples Studied in This Work[a]

label	initial indigo concn (wt %)	heating temp (°C)	indigo content (wt %) for surface/channels	obsd diffraction
SILI-1	0.5	200		mono
SILI-2	1	200	0.5/0.5	mono
SILI-3	2	200	1.1/0.9	mono + indigo
SILI-4	5	200	3.4/0.9	mono + indigo
SILI-5	10	200		mono + indigo
SILI-6	1	230		mono + ortho
SILI-7	5	230		mono + ortho
SILI-8	10	230	3.1/3.2	mono + ortho + indigo
SILI-9	1	300		mono + ortho
SILI-10	5	300	0/4.1	ortho
SILI-11	10	300	1.9/4.2	ortho + indigo
SILI-12	10	230		ortho

[a] All samples, as powders or single crystal (SiLi-12), are heated 5 h at the temperature mentioned. The indigo content is deduced from analysis of the amplitudes of features of the TGA curves at 360−380 °C (departure of surface indigo) and 500−600 °C (departure of indigo incorporated in the zeolite channels). The last column indicates the observed diffracting phase(s): monoclinic (mono), orthorhombic (ortho), and indigo crystals (indigo).

nected with straight channels (5.4×5.6 Å^2) parallel to the *b* axis. MFI zeolites show an orthorhombic-to-monoclinic phase transition, depending on the composition, structural defects, and nature/amount of sorbed molecules (23−25).

The location of cations like tetrapropylammonium (TPA; i.e., the template used in the MFI synthesis protocol) (26) or aromatic molecules such as benzene (27, 28), naphthalene (29), *p*-nitroaniline (30−32), dichlorobenzene (33) and pyridine (34), trapped in an MFI zeolite was studied by different authors mainly using neutron and X-ray diffraction (XRD) techniques and computer simulation. In this study, we combine structural analyses with optical spectroscopies to investigate the indigo@silicalite system. UV−vis fluorescence is sensitive to the structural features of encapsulated dyes, e.g., in zeolite L (35, 36) or $AlPO_4$-5 (37) and MFI (38). Although the fluorescence emission quantum yield of indigo is low (18), fluorescence spectroscopy is a very sensitive tool for determining the distribution of the dye inside and at the surface of the substrate. Roeffaers et al. (39) recently combined electron backscattering diffraction and confocal fluorescence microscopy to map fluorescent reaction products in ZSM-5 crystals.

In this work, we study a new organic−inorganic pigment obtained by mixing and grinding indigo powder with high-silica MFI zeolite. In the absence of foreign atoms, water molecules, or charge-compensated cations in this type of zeolite and given its low concentration of structural defects, we assume that the indigo behavior is driven by a purely siliceous channel structure environment. Insertion into the zeolite is achieved in the solid phase just by heating. The influence of the synthesis parameters (indigo concentration, heating procedure) on the hybrid formation is monitored using optical spectroscopy and XRD techniques. The chromostability of the organic dye in its new "zeolite state" is attested by resistance to irradiation and thermogravimetric analysis (TGA) experiments.

II. EXPERIMENTAL SECTION

II-1. Sample Preparation. The MFI zeolite was prepared at the CRM2, Nancy, France, according to the fluoride route elaborated by Guth et al. (40), which provides crystals of aluminum-free MFI materials with fewer defects than the common hydroxide route (41, 42), using tetrapropylammonium (TPA) cation as a templating agent. The molar composition of the initial synthesis gel was approximately 1:0.08:0.04:20 SiO_2/TPABr/NH_4F/H_2O. This gel was heated at 473 K for 40 days, and then the reaction products were filtered, washed with water, and dried in an oven (43). The purity of the synthesized $(SiO_2)_{96}$ silicalite was confirmed by microprobe analyses. Samples were subsequently calcined at 600 °C in order to eliminate TPA. XRD gives evidence of good crystallization in the monoclinic form, while TGA reveals the low concentration of water and silanols (minor mass loss, less than 1.5 wt % between 25 and 700 °C). A series of MFI samples were prepared as either powders or as single crystals. MFI single crystals have a typical size of $300 \times 150 \times 40$ μm^3 and exhibit a morphology similar to that described by Guth et al. with a typical hourglass pattern (44).

Silicalite powder was mixed with synthetic indigo (from 0.5 to 10 wt %; Aldrich) and finely hand-ground in a mortar. The powder was finally pressed into pellets to enhance contact between the two components. The pellets were heated for 5 h in air at 200, 230, or 300 °C. Doping of single-crystal samples follows the same procedure, omitting the cogrinding step in order to avoid destruction of the single crystals. Table 1 lists samples presented below. This synthesis procedure is inspired by that used for modern reproduction of the Maya Blue pigment (45, 46).

II-2. Techniques. The absorption and diffuse-reflectance spectra (DRUV) were recorded with a double-beam Cary 5000 spectrophotometer (IPREM Pau), in steps of 0.5 nm in the range 400−800 nm using a 1 cm quartz optical cell (Hellma) or an 11-cm-diameter integrating sphere with a custom-made powder holder. The diffuse-reflectance spectra were corrected versus a white standard (Teflon, Aldrich, 55 μm) (47). The DRUV spectra were analyzed according to the Kubelka−Munk model (48), describing light propagation in scattering media with only two parameters, an absorption coefficient, *K*, and an isotropic scattering coefficient, *S* (which both have units of cm^{-1}): $F(R_\infty) = (1 - R_\infty)^2/2R_\infty = K/S = \varepsilon c/S$. With this model based on simple assumptions, the absorption coefficient *K* of the system is proportional to the molar absorption coefficient $\varepsilon(\lambda)$ (L mol^{-1} cm^{-1}) and to the concentration *C* (mol L^{-1}) of the compound.

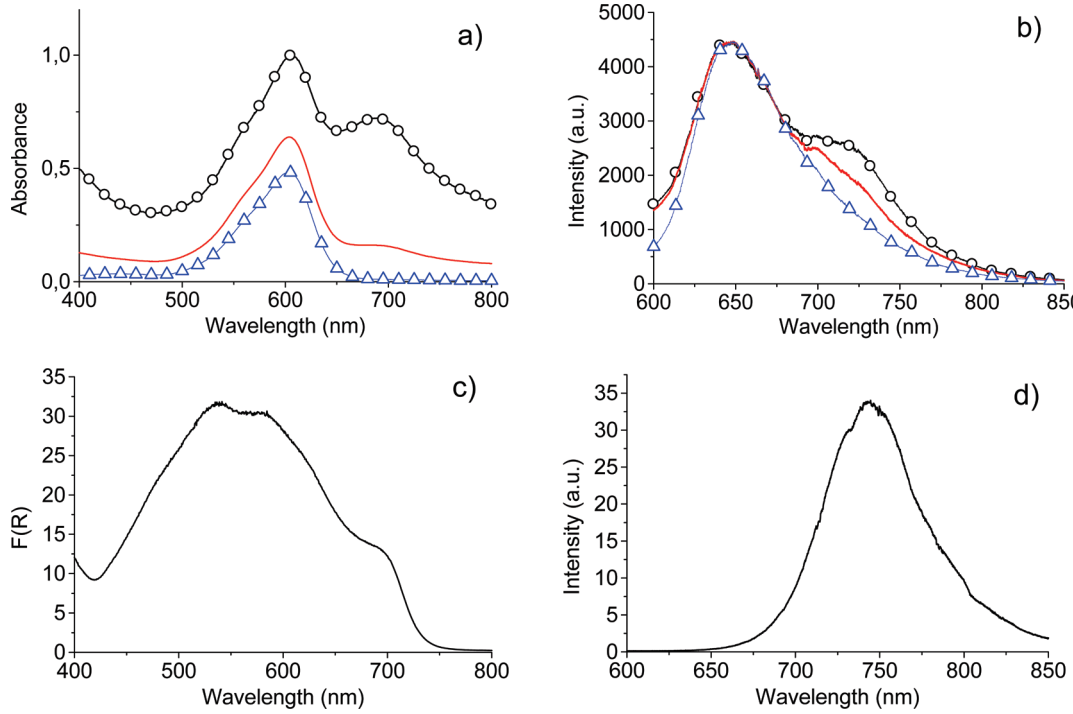

FIGURE 1. Absorption and Kubelka–Munk-scale diffuse-reflectance spectra of indigo. (a) Absorption spectra of indigo in chloroform: (△) 4.1 × 10^{-6} mol L^{-1}; (—) 4.1 × 10^{-5} mol L^{-1}; (○) 1.3 × 10^{-4} mol L^{-1}. l = 1 cm, room temperature. (b) Corresponding fluorescence spectra of indigo in chloroform (λ_{ex} = 488 nm). (c) Kubelka–Munk-scale diffuse-reflectance spectrum of an indigo powder. (d) Fluorescence spectrum of an indigo powder (λ_{ex} = 488 nm).

R_∞ is the reflectance of an "infinite" layer of powder, 4 mm in the present data.

Corrected steady-state emission and excitation spectra were measured using a photon-counting Edinburgh FLS920 fluorescence spectrometer equipped with a xenon lamp (IPREM, Pau, France). Fluorescence spectra of the powdered samples were recorded on powder adhering to sticky tape (negligible fluorescence), in 90° geometry. In situ fluorescence under heating was carried out using a LABRAM Jobin-Yvon Raman spectrometer (LMGP, Grenoble, France) with a LINKAM heating stage. Depth-resolved fluorescence was recorded using focusing of the microscope. The laser power was modulated between 3 mW and 300 μW at the focus.

TGA experiments were conducted on a SETARAM TAG 24 thermoanalyzer instrument (Institut Néel, Grenoble, France). Samples (~15 mg) were heated from 25 to 700 °C at a heating rate of 10 °C min^{-1} under flowing nitrogen.

Powder XRD data were collected in the high-resolution 2θ step scanning mode at the 7-circles diffractometer of Beamline BM02-ESRF (49). The powders were hand-packed in 1 mm capillary glass tubes. Data were processed using the *Fullprof* software (50). In situ modifications of the indigo and zeolite upon heating were followed via two-dimensional diffraction patterns recorded using a CCD detector. Samples were heated in a furnace provided by the Institut Français du Pétrole, which enabled sample oscillation and a homogeneous heating of the capillary (51). The CCD camera was placed 630 mm from the sample at an angle of 12° (2θ). This configuration was used to rapidly achieve sufficient resolution in a particular region of interest during the heating process. Data were analyzed using the Xplot2D application of the *XOP* software package (52). After linearization, a "peak-to-peak" fitting procedure was applied to determine the position, full width at half-maximum, and intensity of each diffraction peak of the ROI. A least-squares refinement was then applied to obtain the cell parameters and volume of the unit cell.

III. RESULTS

III-1. Characterization of Indigo and a Nonheated Indigo/Silicalite Mixture. The UV–vis absorption and fluorescence of indigo depends on the solvent used. The optical absorption of indigo dissolved in chloroform peaks at 606 nm (Figure 1a). At concentrations above 2 × 10^{-5} mol L^{-1}, an additional band appears at 680 nm (Figure 1a). For indigo powder, the diffuse reflectance, shown as Kubelka–Munk transforms, consists of a relatively broad absorption band (Figure 1c). The main components peak at 535, 580, and 680 nm.

The fluorescence of dilute indigo in chloroform appears at ca. 650 nm (Figure 1b). A second band centered at 730 nm appears at a higher indigo concentration (4.1 × 10^{-5} mol L^{-1}). The fluorescence of the indigo crystal powder (Figure 1d) shows a single band at 750 nm.

The Kubelka–Munk-scale diffuse-reflectance spectra of indigo/silicalite mixtures prior to heating are shown in Figure 2a. The principal band peaks at 680 nm for low indigo concentrations. At higher concentration, the relative amplitudes of the bands change and the spectra progressively tend to that of the indigo powder, shown in Figure 1c.

At low indigo concentration (<2 wt %), fluorescence emission occurs at 730 nm (Figure 2b). In addition, weak emission is detected at shorter wavelengths, around 650 nm. When the indigo concentration is increased, the 730 nm fluorescence band shifts to 750 nm and its intensity increases relative to the 650 nm contribution.

Powder XRD analysis shows that the nonheated silicalite/indigo mixture has monoclinic symmetry. The 100, $\bar{1}02$, and 210 indigo reflections are clearly identified on the XRD full

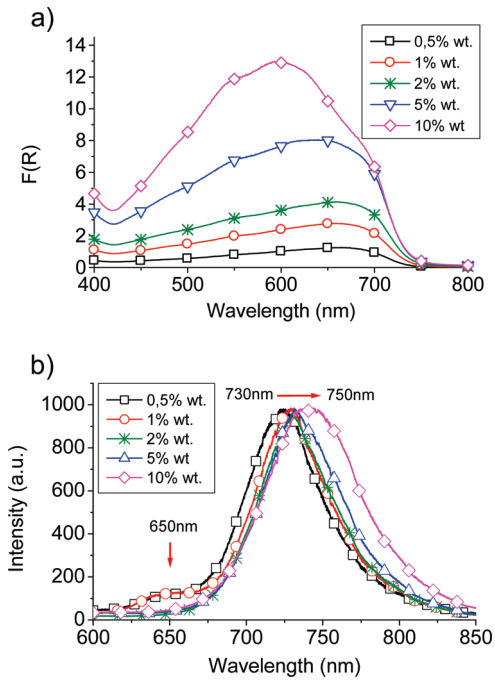

FIGURE 2. Reflectance (a) and fluorescence (b) spectra of unheated indigo/silicalite mixtures versus indigo concentrations. The fluorescence spectra are normalized to 1000 a.u. (λ_{ex} = 488 nm).

pattern of a 5 wt % indigo/silicalite mixture; they are markedly broader than those of the silicalite powder (Figure 3). This supports the presence of small or possibly strained indigo crystallites. The diffraction diagram was refined using two phases (silicalite and indigo) by a full-pattern cell-constrained fitting (50). The refined cell parameters and the corresponding figures of merit are reported in Table 2, in agreement with the previous structural work on MFI single crystals (25, 26) and powder (23) at room temperature.

III-2. Formation of the Indigo@Silicalite Hybrid by Heating. The heat treatment applied to the indigo/silicalite mixture is monitored in situ by fluorescence spectroscopy. An indigo/silicalite mixture is introduced in the heating stage (see the experimental part), and the temperature is progressively increased from 25 to 200 °C (3 °C min^{-1}). At first, only a shift from 750 to 730 nm is observed (Figure 4a). At 200 °C, a second 650 nm band emerges and grows in with time (temperature fixed at 200 °C; Figure 4a).

The relative intensities of the two fluorescence bands (730 and 650 nm) versus depth are shown in Figure 4b, in a silicalite single crystal exposed to indigo vapor at 230 °C for 5 h (SILI-12). The single-crystal *b* axis is parallel to the incident excitation light (inset in Figure 4b). The 730 nm band is maximum when the whole surface of the crystal is illuminated. When the excitation light penetrates further into the crystal, the 650 nm band increases at the expense of the 730 nm band. Therefore, the 730 nm band is clearly due to a surface contribution, while the 650 nm band is due to the bulk colored crystal. Similar results are obtained for different orientations of the single crystal.

The diffuse-reflectance and fluorescence spectra of the 5 wt % indigo@silicalite sample are compared at three different times during the heat treatment (Figure 5a,b): (i) before heating, (ii) in an intermediate state (sample SILI-3, 5 h, 200 °C), and (iii) at the end of the heating process (SILI-10, 5 h, 300 °C). The fluorescence spectrum corresponding to the intermediate state shows two bands at 650 and 730 nm, but only the 650 nm fluorescence band persists in the final state. The diffuse-reflectance bands (Figure 5a) in the 420−570 nm range and at 680 nm (Kubelka−Munk scale) are correlated to the fluorescence band at 730 nm, while the 610 nm band is linked to the 650 nm fluorescence band.

The indigo concentration dependence of the two fluorescence bands for two different heating temperatures (200 and 300 °C) is presented in Figure 5c. The 650 nm fluorescence band [corresponding to a low *I*(730)/*I*(650) value] predominates at a low indigo concentration and/or a higher heating temperature.

Evolution of the indigo@silicalite hybrid has been monitored in situ by XRD (Figure 6). The heating process is shown in Figure 6a. Upon heating, undoped silicalite shows a monoclinic to orthorhombic phase transition around 70 °C (Figure 6b,c), reversible when returning to room temperature. The ferroelastic behavior of the zeolite as a function of the temperature has been discussed previously by other authors (53, 54). At 260 °C, the unit-cell volume of the doped silicalite is not notably affected by the organic dye (Figure 6d). Upon a return to room temperature, the high-temperature orthorhombic phase of the zeolite is maintained (Figure 6b). The broadening of the diffracted peaks when passing from (2) to (3) is due to the presence of an additional room temperature monoclinic phase, in addition to the predominant indigo-induced orthorhombic one.

Depending on the synthesis conditions, the diffraction pattern of the indigo@silicalite samples shows one to three contributions, which come from polycrystalline indigo and the zeolite in varying proportions. The zeolite pattern is easily indexed as monoclinic or orthorhombic. This observation is summarized in Table 1. The full pattern matching of the data yields the lattice parameters, and they are found to be very close to the published data (23, 26) (Table 2). The unit-cell size does not change once the hybrid is formed.

III-3. Stability of the Indigo@Silicalite Hybrids. TGA and calorimetric (DSC) experiments were carried out in order to investigate the thermal stability of the hybrids. The results on silicalite and a 10 wt % indigo@silicalite sample (SILI-8) are presented in Figure 7. Silicalite is subject to minor mass loss below 120 °C, attributable to the departure of physisorbed water (55). Pure indigo powder begins to sublime in the range 250−350 °C before total decomposition at 360 °C (56) (exothermic reaction). SILI-8 exhibits a first mass loss at 360 °C, which corresponds to decomposition of the indigo powder, and a second mass loss in the 550−700 °C range, attributed to the release of indigo sorbed in the silicalite. An exothermic peak (550−700 °C) is correlated with the sorbed molecule decomposition. The powder indigo content and the sorbed indigo content measured by TGA are reported in Table 1 for different hybrid samples.

The indigo@silicalite samples were also exposed to irradiation tests. Fluorescence spectra were recorded for

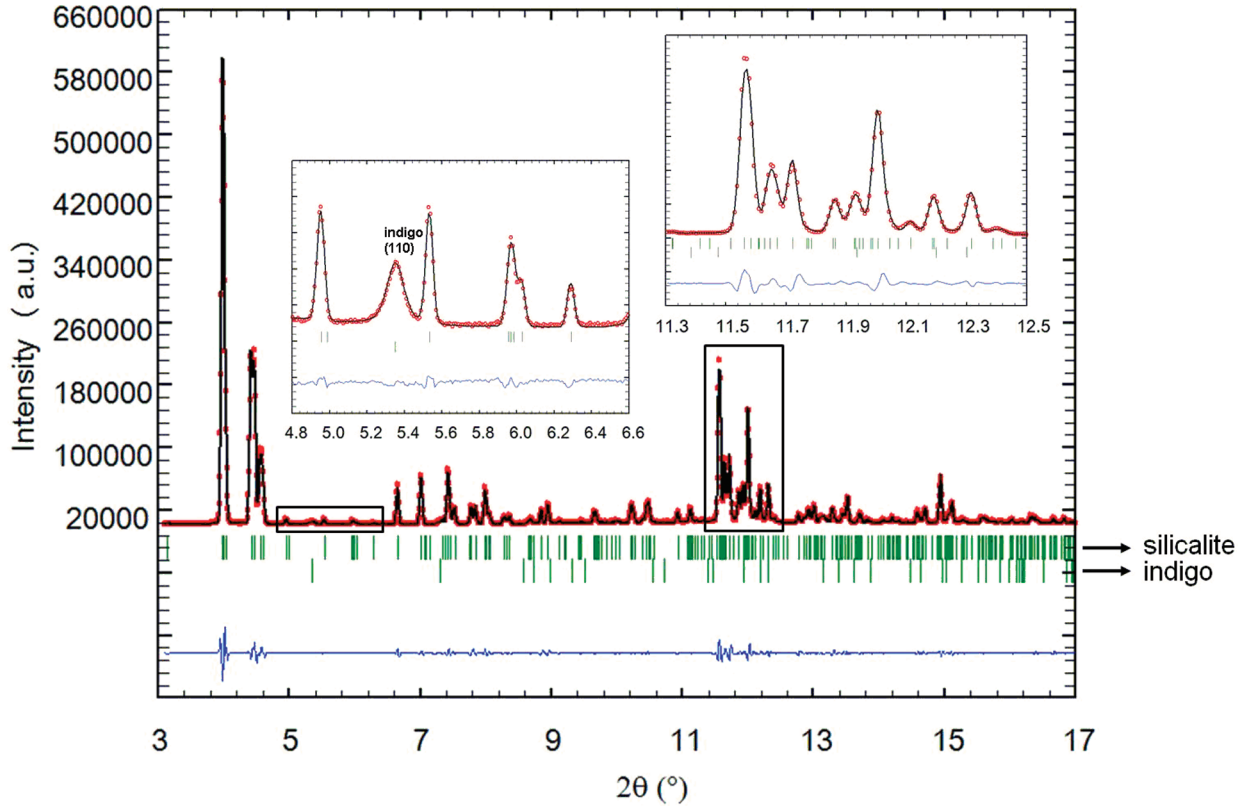

FIGURE 3. XRD full pattern of a 5 wt % indigo/silicalite unheated mixture (red points, experimental data; black line, calculated diagram; green, Bragg positions; blue bottom line, residuals).

Table 2. Crystallographic Results of the Full-Pattern Fitting of Sample SILI-10 (5 wt % Indigo) before and after Heating

	before heating of an indigo/silicalite mixture		after heating of SILI-10	Van Koningsveld et al. (25)	Van Koningsveld et al. (26)
phase	silicalite	indigo	silicalite	ZSM-5 (single crystal)	TPA@ZSM-5 (single crystal)
symetry	monoclinic	monoclinic	orthorhombic	monoclinic	orthorhombic
space group	$P2_1/n$	$P2_1/c$	*Pnma*	$P2_1/n$	*Pnma*
a (Å)	20.0924(3)	10.8762 (6)	20.0301(6)	20.1070(20)	20.0220(20)
b (Å)	19.8620(2)	5.8376(2)	19.8878(6)	19.879(2)	19.8990(20)
c (Å)	13.3446(2)	12.2424(7)	13.3636(4)	13.369(1)	13.383(1)
α (deg)	90.680(1)	90	90	90.67(1)	90
β (deg)	90	130.280(4)	90	90	90
γ (deg)	90	90	90	90	90
volume (Å^3)	5325.1(1)	592.98(5)	5323.5(3)	5343.32	5332.03
R_p (%)	7.52		7.22		
R_{wp} (%)	9.47		9.98		

different laser powers (Figure 8) on SILI-3. The 650 nm band is not notably affected, whereas the 730 nm band, if present, disappears progressively with an increase of the irradiation power. Under similar exposure of pure indigo to the laser beam, the 750 nm fluorescence band of the indigo powder disappears even at low-power irradiation.

IV. DISCUSSION

The optical properties of pure indigo are described in the literature (16, 57−62). The UV−vis absorption is ascribed to the N−H donor to C═O acceptor transition, taking place at the C═C bond central site (63, 64). The transition of indigo from the aggregate state in condensed matter to the monomer state is known to be accompanied by a large blue shift of the fluorescence band (65), as is observed in our spectra (Figure 1). Indeed, Figure 1b shows that the main band of indigo in solution is found at 650 nm, whereas the 730 nm fluorescence band occurs when the molar concentration is increased. Hence, the 650 nm band is assigned to individual molecules, while the 730 nm band is attributed to indigo clusters. Our results also show the correspondence between the 650 nm fluorescence and 606 nm absorbance bands, as well as that between the 730 nm fluorescence and 680 nm absorbance bands.

The changes observed in the two indigo fluorescence bands in indigo@silicalite as a function of the indigo concentration and temperature (Figure 5c) and after irradiation

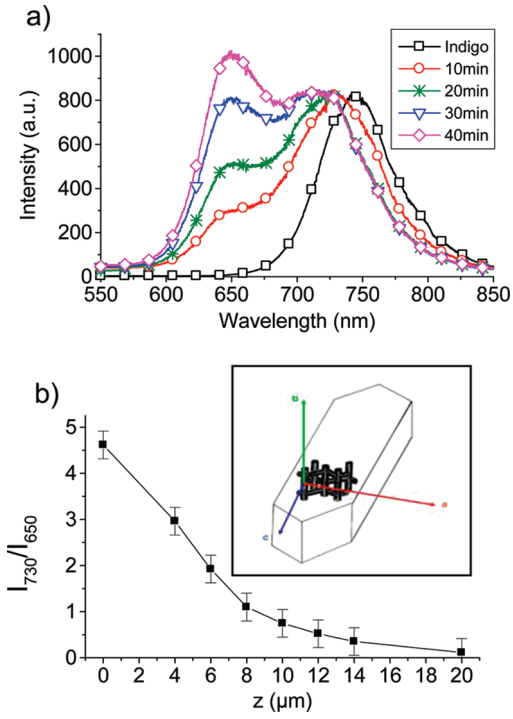

FIGURE 4. Changes of the indigo fluorescence signal versus time (a) and penetration depth (b). (a) In situ fluorescence of a 5 wt % indigo/silicalite mixture heated at 200 °C (λ_{ex} = 488 nm). Spectra are normalized at 730 nm. (b) Fluorescence intensity ratio *I*(730)/*I*(650) in an indigo-doped single crystal from the surface $z = 0$ to 20 μm (λ_{ex} = 488 nm). Inset: crystal axes.

of the pigment formed (Figure 8) clearly suggest the presence of two states of indigo. The fluorescence bands at 650 and 730 nm are assigned to indigo located in the bulk and at the surface of the zeolite, respectively (Figure 4b). Their attribution is justified by a comparison of the fluorescence and UV−vis absorption data of diluted indigo in chloroform and the condensed-state indigo in a crystalline powder (Figure 1) with the data of indigo@silicalite sample (Figure 5d).

The 730 nm fluorescence band in indigo@silicalite (Figure 2b) is present in aggregated indigo (Figure 1b). When the concentration of indigo is increased, the fluorescence emission shifts from 730 to 750 nm. The 750 nm band is assigned to crystalline indigo (Figure 1d). The progressive shift from 750 to 730 nm is attributed to a reduction in the size of the indigo aggregates at the silicalite surface (66). By confrontation with the UV−vis absorption data (Figures 2a and 5a), the 420−570 and 680 nm Kubelka−Munk-scale diffuse-reflectance bands are also assigned to indigo in the condensed state, close to that of the reference indigo powder (Figure 1c). We conclude that powdered indigo lies over the external surface of the zeolite and the degree of aggregation depends on the temperature, heating time, and initial amount of indigo.

The second indigo species is assigned to the fluorescence emission at 650 nm, which predominates upon formation of the complex by heating (Figure 4a). Individual molecules of indigo emit at 650 nm in chloroform (Figure 1b). We interpret the blue shift of the fluorescence band from 730 to 650 nm by the breaking of intermolecular hydrogen bonding and the consequent disaggregation of the indigo powder. Moreover, the origin of the 650 nm band within the bulk of the material is clearly asserted by the depth-resolved fluorescence measurement (Figure 4b). These conclusions are confirmed by the XRD studies (Figure 6). Indeed, the zeolite can be locked into the orthorhombic phase at room temperature, as a consequence of loading with organic sorbates (26, 27, 29, 30). The stabilization at room temperature of the orthorhombic phase of the indigo-doped silicalite can thus be ascribed to the templating effect of indigo inside the zeolite structure. We understand that, upon heating, part of indigo transforms into monomers and enters the zeolite channels; this doping process is responsible for locking of the zeolite structure into its metastable orthorhombic form.

Figure 9 is a schematic representation of the room temperature phase stability of indigo-doped silicalite in $T-C$ space, where T is the heat of formation temperature (5 h, in air in all cases) and C is the initial concentration of the indigo powder in the mixture (see Table 1 for the samples involved). The solid line boundary curve separates the domains in the presence of respectively the one-phase compound (zeolite only) and the two-phase compound. In the latter case, the superimposed powder XRD patterns of both silicalite and indigo are observed. The presence of diffracting indigo is found to correlate with the occurrence of the above-mentioned 730−750 nm fluorescence band, as well as the 420−570 and 680 nm diffuse-reflectance bands. The dashed lines show the occurrence at room temperature of either the monoclinic or orthorhombic symmetry of the indigo@silicalite sample after the heating process, depending again on the temperature of formation and the initial indigo concentration. $T-C$ conditions are stringent for obtaining a single orthorhombic phase after 5 h of baking under atmospheric conditions.

The synthesis of this new hybrid is carried out directly by heating in the solid phase. The procedure to obtain the stable indigo-doped silicalite seems to be easy, but several adjustments are required to ensure homogeneous and reproducible diffusion of indigo. The heating process is a determining factor, and the final temperature has to be carefully monitored. Effective indigo concentrations at the surface and inside the zeolite channels have been checked by TGA for different hybrid samples (Table 1). Heating of the mixture of ground powders of indigo and silicalite at moderate temperatures (below 200 °C) restricts the amount of indigo admitted into the zeolite channels (samples SILI-1 to SILI-5; see Table 1). Too high a temperature increases the mobility of indigo, but indigo is likely to sublime and to diffuse out, as revealed by the significant difference between the initial and final concentrations for samples obtained at 300 °C (Table 1). The fraction of surface indigo can be reduced by increasing the formation temperature of the indigo@zeolite hybrid and by adjusting the initial amount of indigo in the raw mixture. A pure orthorhombic phase is produced in the presence of stable internal indigo, although this structural effect is often incomplete: a mixture of monoclinic and orthorhombic zeolite is more often ob-

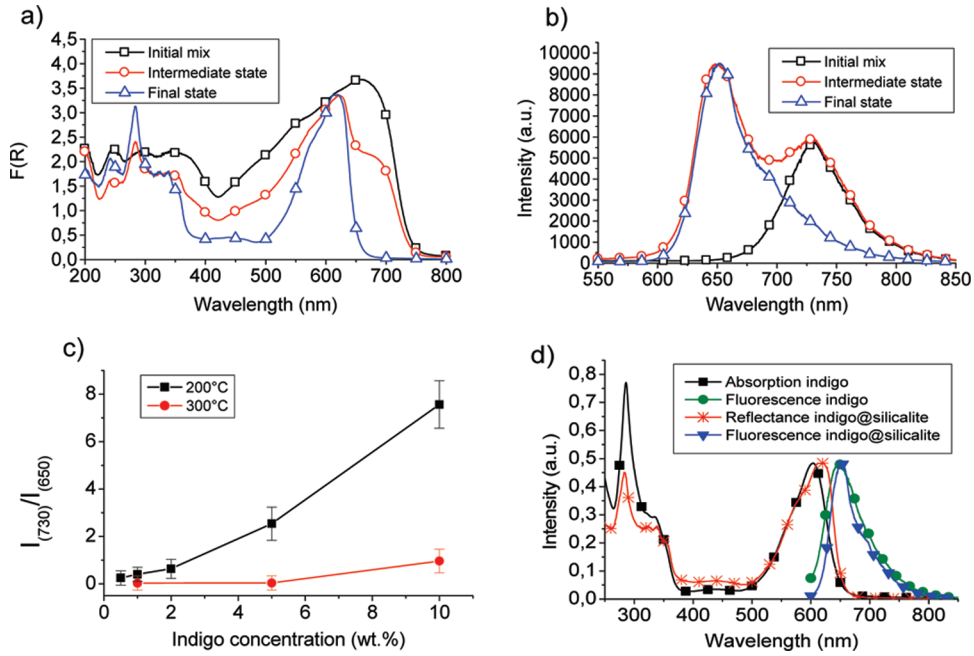

FIGURE 5. Diffuse-reflectance (Kubelka–Munk scale) and fluorescence spectra of the indigo@silicalite hybrids, showing the effect of the indigo concentration and the formation temperature. (a) Kubelka–Munk-scale diffuse-reflectance spectra at three steps of the doping process for a 5 wt % indigo/silicalite sample. (b) Fluorescence spectra at three steps of the doping process for a 5 wt % indigo/silicalite mixture sample. (c) Fluorescence intensity $I(730)/I(650)$ ratio ($\lambda_{ex} = 488$ nm) versus the indigo concentration for two heating temperatures (the same heating time of 5 h). (d) Comparison between the absorption and fluorescence spectra of diluted indigo in $CHCl_3$ and sorbed indigo in silicalite.

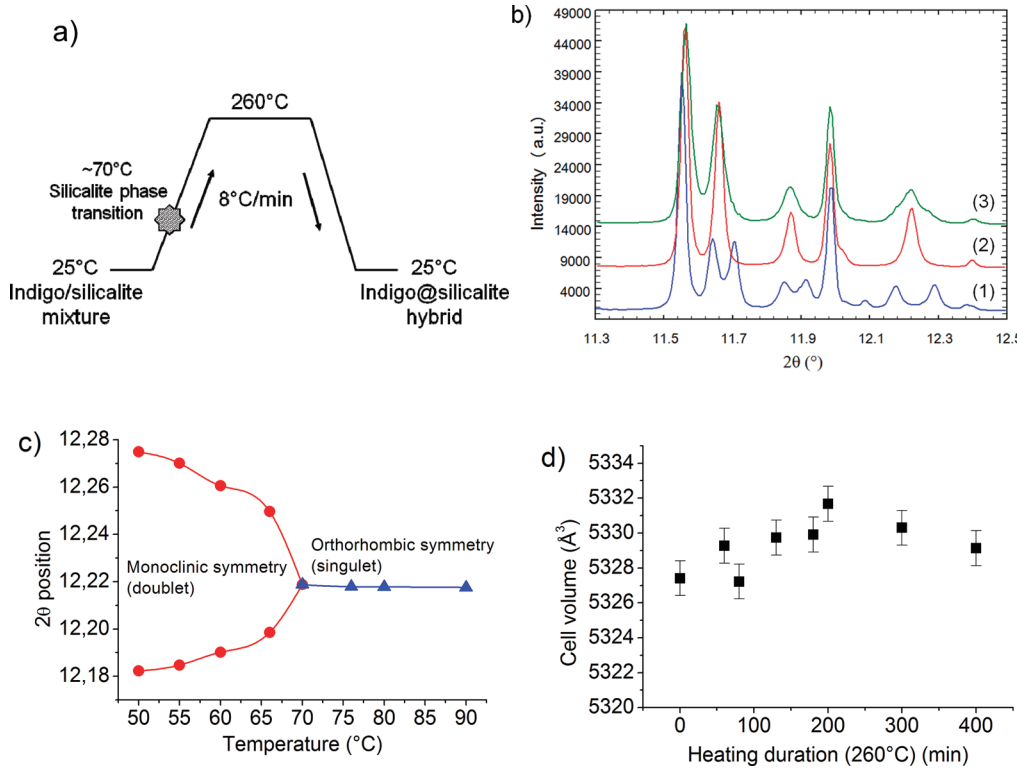

FIGURE 6. XRD results of in situ heating on a 10 wt % indigo/silicalite mixture: (a) temperature cycle; (b) diffraction pattern of the silicalite (1) before heating (monoclinic form), (2) at 260 °C (orthorhombic form), and (3) after a return to room temperature (orthorhombic form). (c) Ferroelastic behavior of the silicalite upon heating. The phase transition occurs at 68 °C. (d) Evolution of the silicalite unit-cell volume at 260 °C.

served. Complete transition is achieved for an initial indigo concentration of 5 wt % and the final temperature of 300 °C (sample SILI-10).

Encapsulation of indigo in an inorganic matrix modifies its color and improves its stability: the color centers (sequestered indigo monomers) are protected against fading pro-

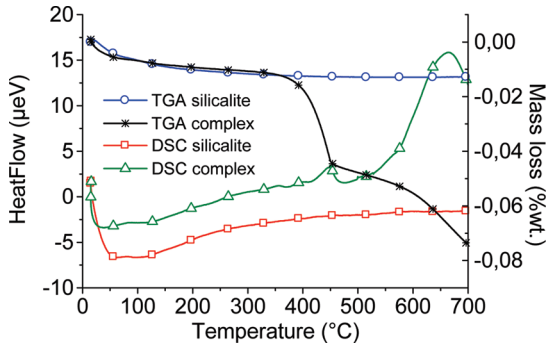

FIGURE 7. TGA/DSC curves recorded on the raw silicalite and SILI-8 sample.

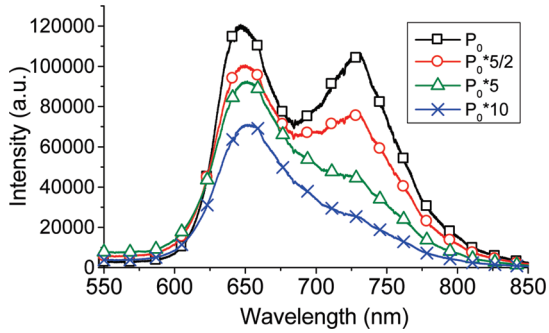

FIGURE 8. Fluorescence spectra of the SILI-3 sample after irradiation (5 min) by a laser (λ_{ex} = 488 nm) at different power levels (P_0 corresponds to a power of 1 μW).

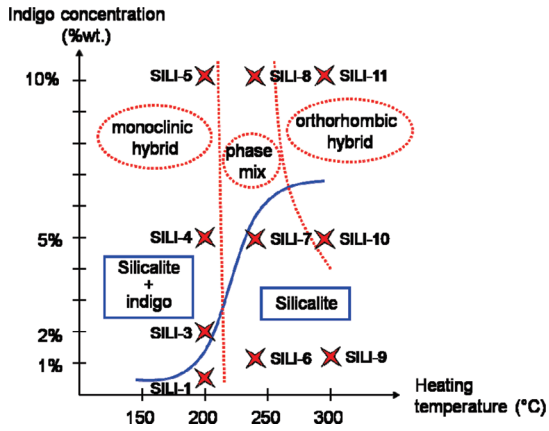

FIGURE 9. Schematic diagram of the silicalite@indigo phase composition as a function of the heating temperature (150−300 °C) and indigo concentrations (0.5−10 wt %).

duced by high temperature (Figure 7) and light (Figure 8). The positions of the diffuse-reflectance and fluorescence bands attributed to monomers of indigo inside the zeolite channels, compared with those of indigo in solution, do not emphasize the formation of any strong organic−inorganic interaction. We believe the high thermal resistance of the indigo@silicalite pigment is related to a particular location of the indigo molecules inside the channels, with the ability to lock the high-temperature phase at room temperature and without the possibility of diffusing out.

The UV−vis diffuse-reflectance spectrum (Figure 5a) accounts for the light-blue color as long as the indigo concentrations are adequate (1 wt %). This color recalls that of ancient Maya Blue, formed by heating palygorskite or sepiolite clays with indigo. In the recent past, Domenech et al. (67) discovered an oxidized form of indigo, dehydroindigo, as a result of the formation process. This is discussed by different groups (68, 69) and could account for the characteristic turquoise shade of Maya Blue. We did not notice such a transformation during the indigo@silicalite synthesis. Nevertheless, the silicalite matrix is really different from the clays used to obtain the archeological pigment, in particular its chemical composition (pure SiO_2), with no possibility of inducing any oxidative reaction. We also compared the high thermal stability of sorbed indigo in silicalite (Figure 7) with that of of the Maya Blue pigment. Ovarlez et al. (70) recently reported the high-temperature stability of indigo molecules trapped in sepiolite tunnels (>380 °C), which is in agreement with our result using the silicalite matrix.

V. CONCLUSION

We have engineered an original indigo@zeolite hybrid composite and studied its structural and spectroscopic properties, which demonstrates a procedure to obtain a durable and resistant pigment. The indigo@silicalite system contains two distinct species of indigo: one is aggregated indigo in contact with the surface of the zeolite, and the second consists of entrapped indigo monomers. The stability of the hybrid pigment is monitored by controlling the initial dye loading and the temperature. The color and color stability directly depend on control of these factors and on the amount of trapped indigo inside the silicalite channels.

The indigo pigment in our study can be thought of as an analogue of the historical pigment Maya Blue (5). The present investigation also suggests that the studied indigo@zeolite hybrid could find applications as a natural, low-cost, and easy-to-make painting material for industrial and artistic use.

Acknowledgment. The TGA experiments were carried out with the help of P. Odier from Institut Néel. J. Kreisel from LMGP provided assistance and support for the fluorescence measurements. N. Boudet, J.-F. Bérar, S. Arnaud, and B. Caillot are thanked for their strong support and advice at the Beamline ESRF/CRG-BM02 for the diffraction measurements. Elemental analyses were performed with the help of Ph. De Parseval at the Laboratory of the Mechanisms and Transfers in Geology, Paul Sabatier University, Toulouse, France. This project is supported by the Région Rhône-Alpes (France) through the CIBLE programme and the Materials for Sustainable Development (MACODEV) consortium.

REFERENCES AND NOTES

(1) Holderlich, W.; Lauth, G.; Wagenblast, G.; Albert, B.; Lamm, G.; Reichelt, H.; Grund, C.; Gruettner-Merten, S. (assigned to W. Holderlich). German Patent DE 4207745, 1992.
(2) Holderlich, W.; Lauth, G.; Muller U.; Brode, S. (assigned to BASF). German Patent DE 4131447, 1992.
(3) Jones, F. N.; Mao, W.; Ziemer, P. D.; Xiao, F.; Hayes, J.; Golden, M. *Prog. Org. Coat.* **2005**, *52*, 9–20.
(4) Diebold, M. P.; Bettler, C. R.; Mukoda, D. M. *J. Coat. Technol.* **2003**, *75*, 29–36.
(5) Van Olphen, H. *Science* **1966**, *154*, 645–646.
(6) Lima, E.; Bosch, P.; Loera, S.; Ibarra, I. A.; Laguna, H.; Lara, V. *Appl. Clay Sci.* **2009**, *42*, 478–482.
(7) Gómez-Romero, P.; Sánchez, C. *New J. Chem.* **2005**, *29*, 57–58.

(8) Sánchez, C.; Ribot, F. *New J. Chem.* **1994**, *18*, 1007–1047.
(9) Sánchez, C.; Julian, B.; Belleville, P.; Popall, M. *J. Mater. Chem.* **2005**, *15*, 3559–3592.
(10) Gettens, R. J. *Am. Antiq.* **1962**, *27*, 557–564.
(11) Kleber, R.; Masschelein-Kleiner, R.; Thissen, J. *Stud. Conserv.* **1967**, *12* (2), 41–56.
(12) Kuang, W.; Facey, G. A.; Detellier, Ch.; Casal, B.; Serratosa, J. M.; Ruiz-Hitzky, E. *Chem. Mater.* **2003**, *15*, 4956–4967.
(13) Chiari, G.; Giustetto, R.; Ricchiardi, G. *Eur. J. Mineral.* **2003**, *15*, 21–33.
(14) Chiari, G.; Giustetto, R.; Druzik, J.; Doehne, E.; Ricchiardi, G. *Appl. Phys. A: Mater. Sci. Process.* **2008**, *90*, 3–7.
(15) Sánchez del Río, M.; Boccaleri, E.; Milanesio, M.; Croce, G.; van Beek, W.; Tsiantos, C.; Chyssikos, G. D.; Gionis, V.; Kacandes, G. H.; Suárez, M.; García-Romero, E. *J. Mater. Sci.* **2009**, *44*, 5524–5536.
(16) Hurry, J. B. *The woad plant and its dye*; Oxford University Press: London, 1939.
(17) Christie, R. M. *Biotech. Histochem.* **2007**, *82*, 51–56.
(18) Seixas de Melo, J.; Moura, A. P.; Melo, M. J. *J. Phys. Chem. A* **2004**, *108*, 6975–6981.
(19) Kokotailo, G. T.; Lawton, S. L.; Olson, D. H.; Meier, W. M. *Nature* **1978**, *272*, 436–437.
(20) Marra, G. L.; Tozzola, G.; Leofanti, G.; Padovan, M.; Petrini, G.; Genoni, F.; Venturelli, B.; Zecchina, A.; Bordiga, S.; Ricchiardi, G. *Stud. Surf. Sci. Catal.* **1994**, *84*, 559–566.
(21) Degnan, T. F.; Chitnis, G. K.; Schipper, P. H. *Microporous Mesoporous Mater.* **2000**, *245*, 35–36.
(22) Wu, E. L.; Lawton, S. L.; Olson, D. H.; Rohrman, A. C., Jr.; Kokotailo, G. T. *J. Phys. Chem.* **1979**, *83*, 2777–2781.
(23) Artioli, G.; Lamberti, C.; Marra, G. J. *Acta Crystallogr.* **2000**, *B56*, 2–10.
(24) Mentzen, B. F. *Mater. Res. Bull.* **1992**, 831–838.
(25) Van Koningsveld, H.; Jansen, J. C.; Van Bekkum, H. *Zeolites* **1990**, *10*, 235–242.
(26) Van Koningsveld, H.; Van Bekkum, H.; Jansen, J. C. *Acta Crystallogr., Sect. B* **1987**, *43*, 127–132.
(27) Goyal, R.; Fitch, A. N.; Jobic, H. *J. Phys. Chem B* **2000**, *104*, 2878–2884.
(28) Klemm, E.; Wang, J.; Emig, G. *Microporous Mesoporous Mater.* **1998**, *26*, 11–21.
(29) Van Koningsveld, H.; Jansen, J. C. *Microporous Mater.* **1996**, *6*, 159–167.
(30) Van Koningsveld, H.; Koegler, J. H. *Microporous Mater.* **1997**, *9*, 71–81.
(31) Gao, F.; Zhu, G.; Li, X.; Li, B.; Terasaki, O.; Qiu, S. *J. Phys. Chem.* **2001**, *B105*, 12704–12708.
(32) Gao, F.; Zhu, G.; Chen, Y.; Li, Y.; Qiu, S. *J. Phys. Chem. B* **2004**, *108*, 3426–3430.
(33) Van Koningsveld, H.; Jansen, J. C.; Van Bekkum, H. *Acta Crystallogr., Sect. B* **1996**, *52*, 140–144.
(34) Nishi, K.; Kamiya, N.; Yokomori, Y. *Microporous Mesoporous Mater.* **2007**, *101*, 83–89.
(35) Megelski, S.; Lieb, A.; Pauchard, M.; Drechsler, A.; Glaus, S.; Debus, C.; Meixner, A. J.; Calzaferri, G. *J. Phys. Chem. B* **2001**, *105*, 25–35.
(36) Busby, M.; Blum, C.; Tibben, M.; Fibikiar, S.; Calzaferri, G.; Subramaniam, V.; De Cola, L. *J. Am. Chem. Soc.* **2008**, *130*, 10970–10976.
(37) Seebacher, C.; Rau, J.; Deeg, F. W.; Braüchle, C.; Altmaier, S.; Jäger, R.; Behrens, P. *Adv. Mater.* **2001**, *13*, 1374–1377.
(38) Karwacki, L.; Stavitski, E.; Kox, M. H. F.; Kornatowski, J.; Weckhuysen, B. M. *Stud. Surf. Sci. Catal.* **2008**, *174*, 757–762.
(39) Roeffaers, M. B. J.; Ameloot, R.; Bons, A. J.; Mortier, W.; De Cremer, G.; De Kloe, R.; Hofkens, J.; De Vos, D. E.; Sels, B. F. *J. Am. Chem. Soc.* **2008**, *130*, 13516–13517.
(40) Guth, J. L.; Kessler, H.; Weg, R. *Proceedings of the 7th lnternational Zeolite Conference*; Elsevier: Amsterdam, The Netherlands, 1986; pp 137−142.
(41) Chézeau, J. M.; Delmotte, L.; Guth, J. L.; Gabelica, Z. *Zeolites* **1991**, *11*, 598–606.
(42) Chézeau, J. M.; Delmotte, L.; Guth, J. L.; Soulard, M. *Zeolites* **1989**, *9*, 78–80.
(43) Aubert, E.; Porcher, F.; Souhassou, M.; Petříček, V.; Lecomte, C. *J. Phys. Chem. B* **2002**, *106*, 1110–1117.
(44) Weidenthaler, C.; Fischer, R. X.; Shannon, R. D.; Medenbach, O. *J. Phys. Chem.* **1994**, *98*, 12687–12694.
(45) Sánchez del Río, M.; Martinetto, P.; Reyes-Valerio, C.; Dooryhée, E.; Suárez, M. *Archaeometry* **2006**, *48*, 115–130.
(46) Domenech, A.; Domenech-Carbo, M. T.; Sánchez del Río, M.; Vasquez de Agredos Pascual, M. L.; Lima, E. *New J. Chem.* **2009**, *33*, 2371–2379.
(47) Weidner, V. R.; Hsia, J. J. *J. Opt. Soc. Am.* **1981**, *71*, 856–861.
(48) Kubelka, P.; Munk, F. *Z. Tech. Phys.* **1931**, *12*, 593–601.
(49) http://www.esrf.eu/UsersAndScience/Experiments/CRG/BM02.
(50) Rodríguez-Carjaval, J. *Physica B* **1993**, *192*, 55–69.
(51) Palancher, H.; Pichon, C.; Rebours, B.; Hodeau, J. L.; Lynch, J.; Bérar, J. F.; Prevot, S.; Conan, G.; Bouchard, C. *J. Appl. Crystallogr.* **2005**, *38*, 370–373.
(52) Sánchez del Río, M.; Dejus, R. J. *SPIE Proc.* **2004**, *5536*, 171–174. (http://ftp.esrf.fr/pub/scisoft/xop2.3/).
(53) Van Koningsveld, H.; Tuinstra, F.; Jansen, J. C.; Van Bekkum, H. *Zeolites* **1989**, *9*, 253–256.
(54) Mentzen, B. F.; Sacerdote-Peronnet, M. *Mater. Res. Bull.* **1993**, *28*, 1017–1024.
(55) Marinkovic, B. A.; Jardim, P. M.; Saavedra, A.; Lau, L. Y.; Baehtz, C.; de Avillez, R. R.; Rizzo, F. *Microporous Mesoporous Mater.* **2004**, *71*, 117–124.
(56) Hubbard, B.; Kuang, W.; Moser, A.; Facey, G. A.; Detellier, C. *Clays Miner.* **2003**, *51*, 318–326.
(57) Bauer, H.; Kowski, K.; Kuhn, H.; Lüttke, W.; Rademacher, P. *J. Mol. Struct.* **1998**, *445*, 277–286.
(58) Perpete, E. A.; Preat, J.; Andre, J. M.; Jacquemin, D. *J. Phys. Chem. A* **2006**, *11*, 5629–5635.
(59) Jacquemin, D.; Preat, J.; Wathelet, V.; Fontaine, M.; Perpete, E. A. *J. Am. Chem. Soc.* **2006**, *128*, 2072–2083.
(60) Jacquemin, D.; Preat, J.; Wathelet, V.; Perpete, E. A. *J. Chem. Phys.* **2006**, *124*, 074104/1−074104/12.
(61) Miliani, C.; Romani, A.; Favaro, G. *Spectrochim. Acta* **1998**, *A54*, 581–588.
(62) Yasarawan, N.; Van Duijneveldt, J. *Langmuir* **2008**, *24*, 7184–7192.
(63) Wille, E.; Lüttke, W. *Angew. Chem., Int. Ed. Engl.* **1971**, *10*, 803–804.
(64) Wyman, G. M. *EPA News Lett.* **1994**, *50*, 9–13.
(65) Monahan, A. R.; Kuder, J. E. *J. Org. Chem.* **1972**, *37*, 4182–4184.
(66) Johnson-Buck, A.; Kim, G.; Wang, S.; Jin Hah, H.; Kopelman, R. *Mol. Cryst. Liq. Cryst.* **2009**, *501*, 138–144.
(67) Doménech, A.; Doménech-Carbó, M. T.; Vázquez de Agredos Pascual, M. L. *J. Phys. Chem. B* **2006**, *110*, 6027–6039.
(68) Tilocca, A.; Fois, E. *J. Phys. Chem. C* **2009**, *113* (20), 8683–8687.
(69) Rondao, R.; Seixas de Melo, J. S.; Bonifacio, V. D. B.; Melo, M. J. *J. Phys. Chem. A* **2010**, *114* (4), 1699–1708.
(70) Ovarlez, S.; Giulieri, F.; Chaze, A. M.; Delamare, F.; Raya, J.; hirschinger, J. *Chem.—Eur. J.* **2009**, *15* (42), 11326–11332.

AM100349B